Argonne National Laboratory

A STUDY OF COOLANT TRANSIENTS DURING A RAPID FISSION-GAS RELEASE IN A FAST-REACTOR SUBASSEMBLY

by

T. C. Chawla and B. M. Hoglund

Printed in the United States of America
Available from
National Technical Information Service
U.S. Department of Commerce
5285 Port Royal Road
Springfield, Virginia 22151
Price: Printed Copy $3.00; Microfiche $0.95

ANL-7651
Reactor Technology

ARGONNE NATIONAL LABORATORY
9700 South Cass Avenue
Argonne, Illinois 60439

A STUDY OF COOLANT TRANSIENTS DURING A RAPID FISSION-GAS RELEASE IN A FAST-REACTOR SUBASSEMBLY

by

T. C. Chawla and B. M. Hoglund*

Reactor Analysis and Safety Division

January 1971

*Now with the Center for Environmental Studies

TABLE OF CONTENTS

	Page
NOMENCLATURE	8
ABSTRACT	9
I. INTRODUCTION	9
II. EXPERIMENTAL APPARATUS	12
III. A TYPICAL TRANSIENT	15
IV. THE MATHEMATICAL MODEL	17
A. General Considerations	17
1. Governing Equations for Liquid Phase	17
2. Governing Equations for Gas Phase	18
B. Application to Reactor Configuration and Conditions	19
1. Motion of the Upper Gas-Liquid Interface	20
2. Inertial Contribution of Fluid in the Exit Plenum	21
3. Motion of Lower Gas-Liquid Interface	22
4. Inertial Contribution of Fluid in the Inlet Plenum	23
5. Resolution of Equations for Gas Bubble	23
C. Application to Water Out-of-Pile Configuration and Conditions	25
V. QUANTITATIVE CRITERION FOR VALID APPLICATION OF THE ANALYTICAL MODEL	27
VI. COMPUTATIONS AND DISCUSSION OF RESULTS	29
A. The Water Out-of-Pile Simulation Loop	29
B. Reactor Configuration and Conditions	37
VII. CONCLUSIONS	39
ACKNOWLEDGMENTS	40
REFERENCES	41

LIST OF FIGURES

No.	Title	Page
1.	A View of the Experimental Arrangement.	12
2.	Schematic Diagram of Gas-release Assembly	13
3.	Schematic Diagram of Water-circulation Loop	14
4.	Schematic Diagram of Layout of Instrumentation	14
5.	Strip-chart Record for a Typical Transient	15
6.	Sequence of Bubble Expansion at Various Time Intervals for Typical Transient	16
7.	Description of Coordinate System for Reactor-subassembly Configuration	20
8.	Description of Coordinate System for Water Out-of-Pile Loop Configuration	25
9.	Measured Distribution of Pressure-loss Coefficient of Variable Constriction (valve) in the Bypass as a Function of Steady-state Bypass Flow	29
10.	Variation of Pressure at Exit of Pump with Pump Capacity . . .	29
11.	Comparison between Experimental and Predicted Displacements of Upper and Lower Gas-Liquid Interfaces for Initial Test Conditions: Coolant Velocity = 30 fps; Gas-plenum Pressure = 515.0 psia; Breach Size = 0.063-in. Diameter . . .	31
12.	Comparison between Experimental and Predicted Displacements of Upper and Lower Gas-Liquid Interfaces for Initial Test Conditions: Coolant Velocity = 30 fps; Gas-plenum Pressure = 1000.0 psia; Breach Size = 0.063-in. Diameter. . .	31
13.	Comparison between Experimental and Predicted Displacements of Upper and Lower Gas-Liquid Interfaces for Initial Test Conditions: Coolant Velocity = 28.0 fps; Gas-plenum Pressure = 665.0 psia; Breach Size = 1/16 x 1/8 in.^{2}	31
14.	Comparison between Experimental and Predicted Displacements of Upper and Lower Gas-Liquid Interfaces for Initial Test Conditions: Coolant Velocity = 28.0 fps; Gas-plenum Pressure = 995.0 psia; Breach Size = 1/16 x 1/8 in.^{2}	31
15.	Comparison between Experimental and Predicted Displacements of Upper and Lower Gas-Liquid Interfaces for Initial Test Conditions: Coolant Velocity = 18.0 fps; Gas-plenum Pressure = 665.0 psia; Breach Size = 1/16 x 1/8 in.^{2}	32

LIST OF FIGURES

No.	Title	Page
16.	Comparison between Experimental and Predicted Displacements of Upper and Lower Gas-Liquid Interfaces for Initial Test Conditions: Coolant Velocity = 18.0 fps; Gas-plenum Pressure = 835.0 psia; Breach Size = 1/16 x 1/8 in.^{2}	32
17.	Temporal Variation of Pressure in Gas Plenum during Gas Discharge for Initial Test Conditions: Coolant Velocity = 30.0 fps; Breach Size = 0.063-in. Diameter	33
18.	Temporal Variation of Pressure in Gas Plenum during Gas Discharge for Initial Test Conditions: Coolant Velocity = 28.0 fps; Breach Size = 1/16 x 1/8 in.^{2}	33
19.	Temporal Variation of Pressure in Gas Plenum during Gas Discharge for Initial Test Conditions: Coolant Velocity = 18.0 fps; Breach Size = 1/16 x 1/8 in.^{2}	33
20.	Temporal Distribution of Pressures at Various Locations in Test Section for Initial Test Conditions: Coolant Velocity = 30.0 fps; Gas-plenum Pressure = 1000.0 psia; Breach Size = 0.063-in. Diameter	34
21.	Temporal Distribution of Pressures at Various Locations in Test Section for Initial Test Conditions: Coolant Velocity = 28.0 fps; Gas-plenum Pressure = 995.0 psia; Breach Size = 1/16 x 1/8 in.^{2}	34
22.	Temporal Distribution of Pressures at Various Locations in Test Section for Initial Test Conditions: Coolant Velocity = 18.0 fps; Gas-plenum Pressure = 835.0 psia; Breach Size = 1/16 x 1/8 in.^{2}	34
23.	Predicted Temporal Distribution of Pressures at Various Locations in Loop for Initial Test Conditions: Coolant Velocity = 30 fps; Gas-plenum Pressure = 1000.0 psia; Breach Size = 0.063-in. Diameter	35
24.	Predicted Temporal Distribution of Pressures at Various Locations in Loop for Initial Test Conditions: Coolant Velocity = 28.0 fps; Gas-plenum Pressure = 995.0 psia; Breach Size = 1/16 x 1/8 in.^{2}	35
25.	Predicted Temporal Distribution of Pressures at Various Locations in Loop for Initial Test Conditions: Coolant Velocity = 18.0 fps; Gas-plenum Pressure = 835.0 psia; Breach Size = 1/16 x 1/8 in.^{2}	36

LIST OF FIGURES

No.	Title	Page
26.	Predicted Temporal Variation of Flow for Initial Test Conditions: Coolant Velocity = 30 fps; Gas-plenum Pressure = 1000.0 psia; Breach Size = 0.063-in. Diameter	36
27.	Predicted Temporal Variation of Flow for Initial Test Conditions: Coolant Velocity = 28.0 fps; Gas-plenum Pressure = 995.0 psia; Breach Size = 1/16 x 1/8 $in.^2$	36
28.	Predicted Temporal Variation of Flow for Initial Test Conditions: Coolant Velocity = 18.0 fps; Gas-plenum Pressure = 835.0 psia; Breach Size = 1/16 x 1/8 $in.^2$	36
29.	Calculated Displacements of Upper and Lower Gas-Liquid Interfaces for FFTF Fuel Subassembly for Initial Conditions: Coolant Velocity = 25.5 fps; Gas-plenum Pressure = 1000.0 psia	38

NOMENCLATURE

A	Cross-sectional area of flow path
A_c	Effective cross-sectional area of fuel assembly for flow
A_{cc}	Cross-sectional area at junction point C (see Fig. 8)
A_0	Area of breach
A_{0i}	Area of breach in pin i
a	Radius of equivalent plenum (portion of plenum associated with a single subassembly)
b	Radius of transition piece (or outlet region)
C_d	Coefficient of discharge
C_p	Specific heat of gas at constant pressure
C_v	Specific heat of gas at constant volume
C_{di}	Coefficient of discharge for breach in pin i
D	Diameter of flow path
D_h	Hydraulic diameter of fuel assembly
f	Friction factor
f_L	Friction factor for lower liquid slug in fuel assembly
f_u	Friction factor for upper liquid slug in fuel assembly
g	Acceleration due to gravity
g_c	Dimensional conversion factor
H	Height of liquid in exit plenum
h	Film heat-transfer coefficient between bubble and surroundings
H_L	Length of transition piece (outlet region)
$I(t - t_i)$	Unit step function $\begin{cases} 0 \text{ for } t < t_i \\ 1 \text{ for } t \geq t_i \end{cases}$
J	Mechanical equivalent of heat
$J_\ell(\alpha_n r)$	Bessel function of the first kind of order ℓ
k	Number of pins that fail at $t = 0$
K_c	Pressure-loss coefficient for sudden contraction at inlet to fuel assembly
K_E	Pressure-loss coefficient for sudden expansion at section E-E (see Fig. 8)
K_G	Pressure-loss coefficient for grid
K_T	Combined pressure-loss coefficient for total flow orifice and energy loss due to gradual contraction at conjunction point C (see Fig. 8)
K_{bE}	Pressure-loss coefficient for sudden expansion at junction of bypass and exit plenum
K_{bp}	Pressure-loss coefficient for bypass valve opening
K_{or}	Pressure-loss coefficient for orifice in inlet piece
L	Length of fuel assembly
L_{bH}	Length of horizontal section of bypass pipe
L_{bV}	Length of vertical section of bypass pipe
L_{IH}	Length of horizontal section of inlet piece
L_{IV}	Length of vertical section of inlet piece
L_{TH}	Length of horizontal section of total-flow pipe
L_{TV}	Length of vertical section of total-flow pipe
m,n	Constants in Eq. 3
N	Number of pins ruptured
P_a	Pressure at top of exit plenum
P_b	Pressure in gas bubble at any time t
P_C	Pressure at point C (see Fig. 8)
P_D	Pressure at point D (see Fig. 8)
P_E	Pressure at section E-E (see Fig. 8)
P_{AT}	Pressure at exit of pumps or at inlet of inlet plenum
P_{b0}	Pressure in gas bubble at $t = 0$
P_{gi}	Pressure in gas plenum i at any time t
P_{g0}	Pressure in gas plenum at $t = 0$
Q_i	Mass rate of discharge of gas from plenum i
R	Gas constant
S	Heat-transfer surface area between bubble and surroundings
t	Time
t_i	Rupture time of a pin i
t_r	Initial transit time of coolant for single pass through fuel assembly
T_b	Temperature of gas in gas bubble
T_{gi}	Temperature of gas in gas plenum at any time t
T_{g0}	Temperature of gas in gas plenum at $t = 0$
ΔT	Temperature difference between bubble and surroundings
U_0	Initial coolant velocity in fuel subassembly
u	Velocity of coolant
u_c	Velocity of upper gas-liquid interface
u_L	Velocity of lower gas-liquid interface
V	Volume of gas plenum
V_b	Volume of gas bubble at any time t
V_{b0}	Volume of gas bubble at $t = 0$
x	Axial coordinate
X_L	Position of lower gas-liquid interface
X_u	Position of upper gas-liquid interface
X_{L0}	Initial position of lower gas-liquid interface
X_{u0}	Initial position of upper gas-liquid interface

Greek Letters

α	Constant in Eq. 16
β	Constant in Eq. 29
γ	Ratio of specific heat at constant pressure to specific heat at constant volume
ρ	Density of coolant
ρ_b	Density of gas in bubble at any time t
ρ_{b0}	Density of gas in bubble at $t = 0$
ρ_{gi}	Density of gas in gas plenum i at any time t
ρ_{g0}	Density of gas in gas plenum at $t = 0$

Subscripts

bp	Bypass flow
I	Inlet piece
IP	Inlet plenum
p	Exit plenum
T	Total-flow pipe or main pipe
Tr	Transition piece (outlet region)

A STUDY OF COOLANT TRANSIENTS DURING A RAPID FISSION-GAS RELEASE IN A FAST-REACTOR SUBASSEMBLY

by

T. C. Chawla and B. M. Hoglund

ABSTRACT

Flow transients initiated by rapid gas release were studied both experimentally and analytically. The mathematical model developed was used to consider a multiple pin failure in a fast-reactor subassembly. In formulating the model, it was assumed that the released gas filled the subassembly cross section uniformly and that the coolant flow was incompressible. The inertial contribution of the liquid columns beyond the pin assembly, as well as the three-dimensional flow effects in the inlet and outlet plenums, were considered. In the application of the model to out-of-pile simulation loops or in-pile test loops, points of departure in hydraulic simulation of the actual reactor conditions can be taken into account. A quantitative criterion for valid application of the model was obtained in terms of breach size, number of pins ruptured, initial gas-plenum pressure and temperature, and subassembly operating conditions. The predictions of the flow transients obtained by means of the model agreed well with the experimental data. An example of the application of the model to a reactor configuration was given using an FFTF fuel subassembly.

I. INTRODUCTION

In the investigation of the phenomenology of failure propagation resulting from a release of fission gas from a ruptured fuel pin, it is convenient to define three regimes of gas release rates. The first regime pertains to those failures that result in a very rapid release of gas and may cause failure propagation by (1) thermal insulation of the adjacent pins as a result of coolant transients that temporarily void the region and/or (2) generation of the pressure pulses due to the initial burst of high-pressure gas into a low-pressure coolant. The second regime covers somewhat slower (than the above-described rapid gas release) rates of gas release that produce a persistent gas jet. The phenomena associated with this regime of gas release has been studied experimentally by Hoglund *et al.*[1] using a single

heated channel in an out-of-pile water loop. They found for water as a coolant that the gas jet entrains liquid drops and produces spray cooling. The third regime covers still slower rates of gas release. In this regime, the postulated mode of propagation is overheating of pins due to local flow reduction produced by the two-phase flow characteristics of fission gas and sodium mixture.

The present study is aimed at investigating both experimentally and analytically the phenomena associated with the first regime, i.e., the rapid gas release (neglecting the resistance to the flow of gas internally in the fuel or assuming a breach occurring in the vicinity of gas plenum region).

As mentioned above, the rapid gas release could result in overheating of the cladding due to voiding of the region, or the adjacent fuel pins may be ruptured due to excessive deflection caused by the pressure pulses traveling radially from the rupture point. The sudden release of fission gas causes almost complete separation of the liquid column in the fuel subassembly into two parts in such a way that the lower liquid column experiences a rapid deceleration and the upper liquid column is rapidly accelerated. The rapidity of these flow transients results in generation of pressure pulses of considerable intensity and width. In a recent experiment performed by Koenig,[2] these pressure pulses have resulted in some deformation of the hexagonal can containing the fuel assembly.

In addition to pin-to-pin failure propagation as implied in the above description, the results of analysis indicate there exists a very definite possibility that in a multiple pin failure, where a considerable amount of fission gas may be ejected into a subassembly, the coolant flow in the lower liquid column would be reversed. A quantity of gas which makes its way into the inlet plenum would then enter other adjacent subassemblies. Reduction of coolant flow in the affected adjacent fuel assemblies would result due to the increased friction factor of the two-phase flow mixture. Hori and Friedland's one-dimensional analysis of the problem[3] indicates that the ratio of the flow reduction (original flow rate minus the reduced flow rate) to the original flow is approximately equal to void fraction of the two-phase mixture. The temperature transients caused by the entrance of a two-phase mixture in adjacent subassemblies may result in propagation of failure to other subassemblies. In addition, the voiding caused by fission gas entering adjacent subassemblies may cause reactivity effects.

An analysis of the rapid gas release was made by Hori and Friedland[4] in which they assumed that the ejected gas forms a single cylindrical bubble and subsequently expands isothermally, thereby expelling the coolant from the subassembly. Their calculation model is basically a "piston model," which has been extensively employed in calculation of voiding rates due to sudden vaporization of a superheated coolant in a reactor fuel assembly.[5-8] Hori and Friedland also compared the results of their calculations with

out-of-pile water loop test data.[9] They found that the experimental bubble size and blanketing time were about twice the calculated values. They attributed this discrepancy to mixing of the phases and to differences between the test and calculation conditions.

Recently Kondo et al.[10] performed two preliminary simulation experiments in out-of-pile water loops. The first experiment simulated a persistent gas jet impinging on a single heated pin. They found that the cladding surface temperature dropped sharply at the point of gas jet impingement. These findings are in agreement with more recently reported work of Hoglund et al.,[1] who also found that the most dominant mode of heat transfer at the point of gas-jet impingement is spray cooling with liquid entrained in the jet as it penetrates the coolant. The second experiment of Kondo et al. simulated a sudden burst of gas from the central pin of the 64-pin assembly. They found that the hydraulic transients are very rapid and are accompanied by generation of pressure pulses of about 100 psi. Their calculation model for rapid gas release is identical to that by Hori and Friedland.[4] They suggested that any lack of agreement between the calculations and the data arises from their choice of boundary conditions, which included a fixed inlet pressure.

In an effort to develop an adequate predictive analytical capability, it was clear from a review of existing investigations of a rapid gas release that additional experiments were required to provide more detailed information on the phenomenon involved. In addition, an adequate definition of the conditions for which an analytical model was valid was needed. It was also evident that points of departure in hydraulic simulation of actual reactor configuration and conditions should be adequately accounted for in a calculational model. These include (i) limited bypass flow because of the limited capacity of the available pumps in a simulation loop (nonconstancy of the pressure drop across the test section during the transients) and (ii) the inertial lengths beyond the ends of the pin assembly.

Specifically then, the objectives of the present study are: (1) to provide quantitative data regarding hydraulic transients, (2) to study the effect of variables such as (a) gas-plenum pressure, (b) rates of coolant flow, and (c) type and size of the cladding breach (holes and slots), (3) to observe intensity and half-width of the pressure pulses, and (4) to formulate an analytical model consistent with the experimental observations and conditions.

II. EXPERIMENTAL APPARATUS

The experiments were performed in a test section consisting of a triangular array of 19 pins enclosed in a Plexiglas channel. The pin bundle consisted of 18, 1/4-in.-OD x 71, 1/2-in.-long, wire-wrapped Plexiglas rods surrounding a central, hollow, stainless steel tube, also of 1/4-in. OD. The spacer wire was of 0.05-in. diameter and was wrapped on pins with a 12-in. pitch. The whole pin bundle was supported at the bottom by a perforated grid plate. The Plexiglas section was made in two halves which, when bolted together with O-ring sealing between them, had a hexagonal internal cross section. On the outside, the section was rectangular to minimize refraction in viewing the flow regimes inside the section. The whole assembled section was reinforced with four long bolts and two end plates, and was mounted vertically, as shown in Fig. 1.

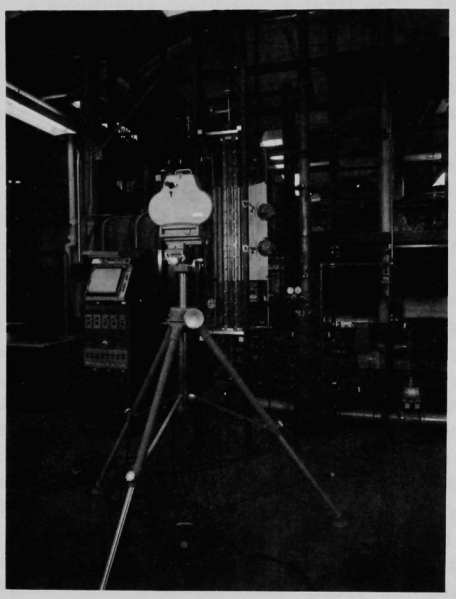

Fig. 1. A View of the Experimental Arrangement. ANL Neg. No. 113-2572.

To simulate the release of fission gas, the central tube had a predrilled orifice and was fitted with a pressure-actuated valve which allowed repeated gas-release tests without disassembly of the test section. The valve system was installed inside the stainless steel tube such that it divided the length of tube into a gas plenum with a fixed volume of 0.75 cu in. at the top and a gas-supply section in the bottom. (The details of this assembly are shown in Fig. 2.) The gas reservoir was instrumented with a small, dynamic pressure transducer. The gas-supply section in the lower half of the tube contained an end fitting for entrance of the gas-supply tube. The internal end of the gas-supply tube was fitted with an adapter to accommodate the detent of the piston assembly. The only moving component was the small piston-valve assembly which was fitted with two O-ring seals, one on the top end and the other in the middle of the piston length. The gas reservoir was charged by applying gas pressure from the supply, which moved the piston to the closed position. The gas then slowly leaked through the central hole (made by machining a flat on the piston pin) until the pressure on both sides was equal. To initiate gas release, the pressure in the supply line was vented through a solenoid-valve system. As a result, the pressure forces on the piston became

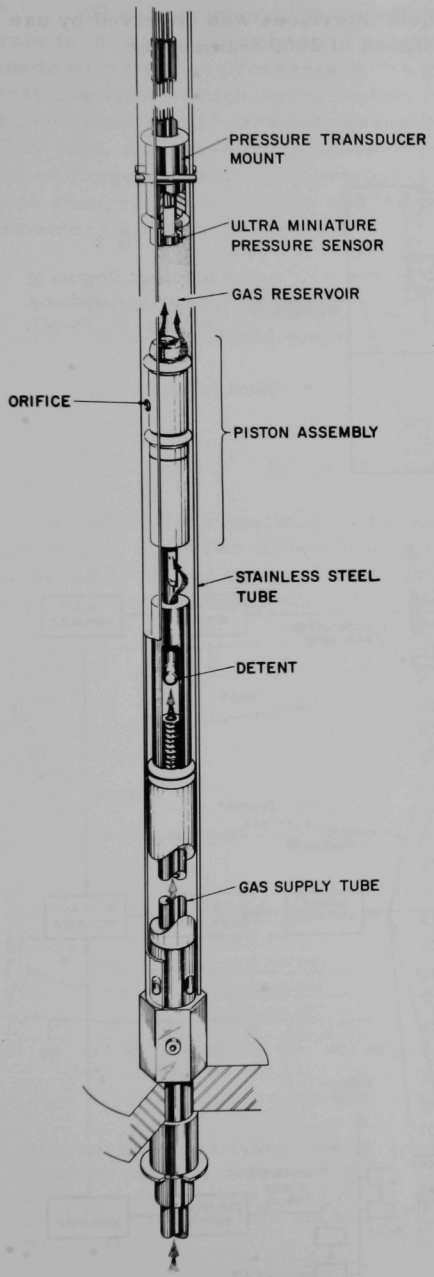

unbalanced, and the pressure in the top gas reservoir (plenum) quickly moved the piston to expose the orifice in the tube wall. To repeat the experiment, the vent in the supply was closed and the supply pressure was applied again.

The schematic diagram of the water-circulation loop, in which the 19-pin test section is installed, is shown in Fig. 3. The water for the coolant to the test section was supplied by two pumps, each of approximately 150-gpm capacity at a discharge pressure of 90 psia. A bypass flow channel was placed in parallel with the test section to simulate the flow paths in the reactor core. The flow rate through the test section was varied by controlling the bypass-valve opening. The water was maintained at room temperature (~70°F) throughout the experiment.

The test section was instrumented with several piezoelectric, dynamic pressure transducers located at various axial positions along the test section. These transducers were provided to record transient pressures produced by the sudden release of gas from the orifice located in the wall of the central stainless steel tube. Two Heise gauges were also provided to measure the system inlet and outlet pressures under steady-state conditions. The flow rate to the test section was measured by a strain gauge type of differential pressure transducer placed across an orifice. The associated recording instruments are

Fig. 2

Schematic Diagram of Gas-release Assembly. ANL Neg. No. 113-3221.

shown in Fig. 4. The motion of gas-liquid interfaces was observed by use of a high-speed camera operating at a speed of 2000 frames/sec.

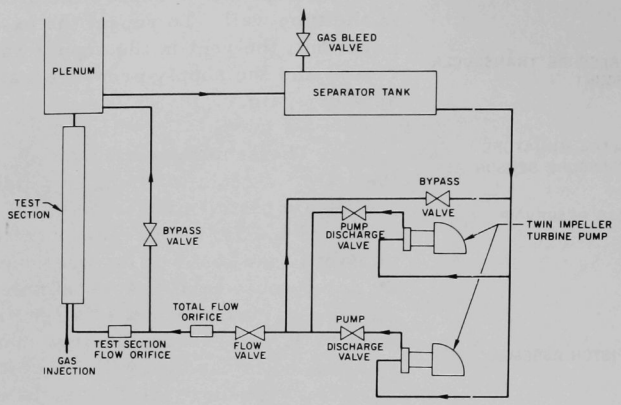

Fig. 3

Schematic Diagram of Water-circulation Loop. ANL Neg. No. 900-557.

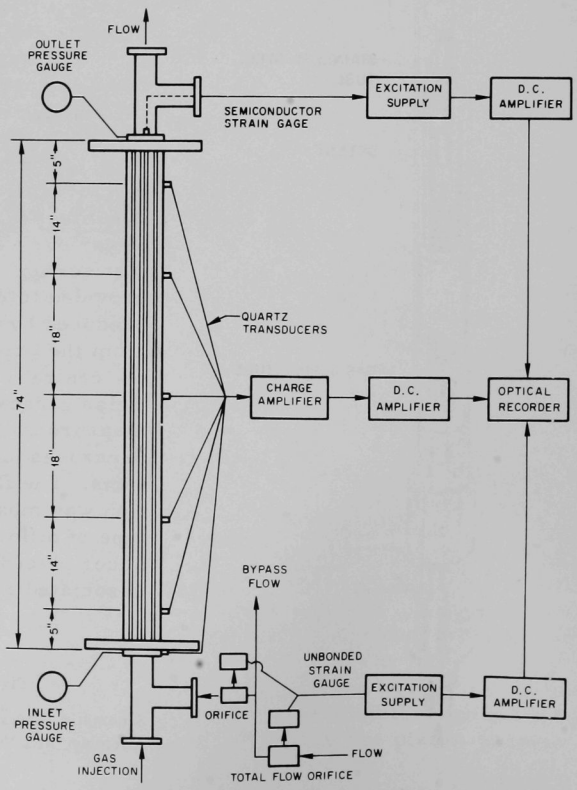

Fig. 4

Schematic Diagram of Lay-out of Instrumentation. ANL Neg. No. 900-554.

The experimental procedure consisted of setting the desired flow rate in the test assembly and the bypass channel. A series of runs were made with various pressures in the gas plenum. The data obtained for each test consisted of high-speed motion pictures to observe the motion of the bubble interfaces, transient pressures at various axial locations, transient flow rate, and gas-plenum pressure. After data were obtained for the desired range of gas-plenum pressures, the flow rate through the test section was changed to a new value and the tests were repeated. The range of parameters for these tests were:

Coolant velocity	18, 30 fps
Gas-plenum pressure	500, 1000 psia
Breach size and shape	0.063-in.-dia hole
	$1/16 \times 1/8$-in.^{2} slot
Location of breach	Center of rod bundle

III. A TYPICAL TRANSIENT

Prior to formulation of the mathematical model, it would be to our advantage, for better understanding of the phenomenon involved, to consider a typical transient initiated by rapid gas release. Results pertaining to a typical transient are given in Figs. 5 and 6. Figure 5 indicates that the flow into the test section is rapidly (in about 35 msec) reduced from about 28 to about 21 fps and then gradually recovers its original value, accompanied by an overshoot in about 115 msec. The gas from the gas plenum is discharged almost completely in a very short time (about 40 msec). The peak pressure pulse measured at the wall of the test section at its midplane has a maximum intensity of approximately 100 psi above the local system pressure and a half-width of about 15 msec. The intensity of these pressure pulses falls off quickly along the length of the test section (e.g., the peak value measured in the transient shown in Fig. 5 is about 60 psi above the local system pressure just above the grid and about 20 psi below the grid). Figure 6 shows a typical flow pattern at various time intervals; it is clear that the ejected gas expands radially to occupy the entire cross section at the point of the release and then expands axially as a single bubble.

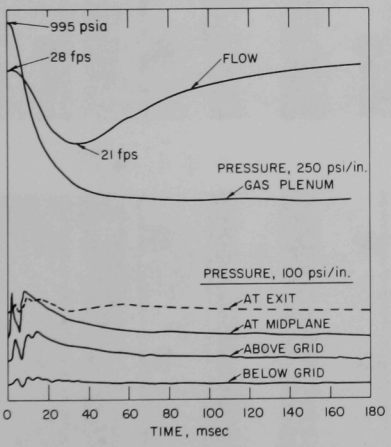

Fig. 5

Strip-chart Record for a Typical Transient (initial test conditions: coolant velocity = 28.0 fps; gas-plenum pressure = 995.0 psia; breach size = $1/16 \times 1/8$ in.^{2}). ANL Neg. No. 900-562.

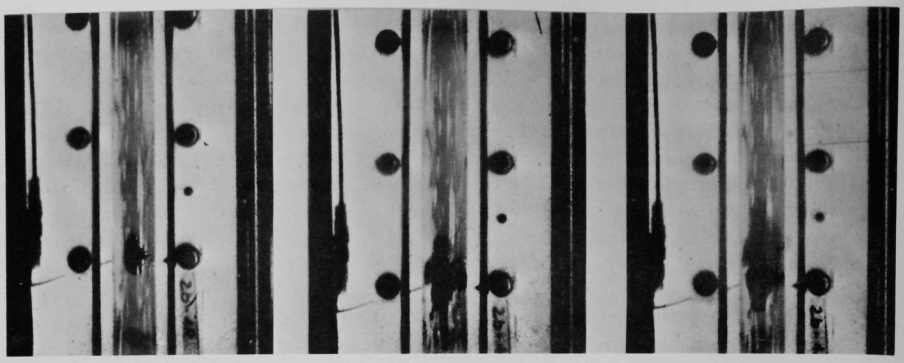

0 msec 1 msec 2 msec

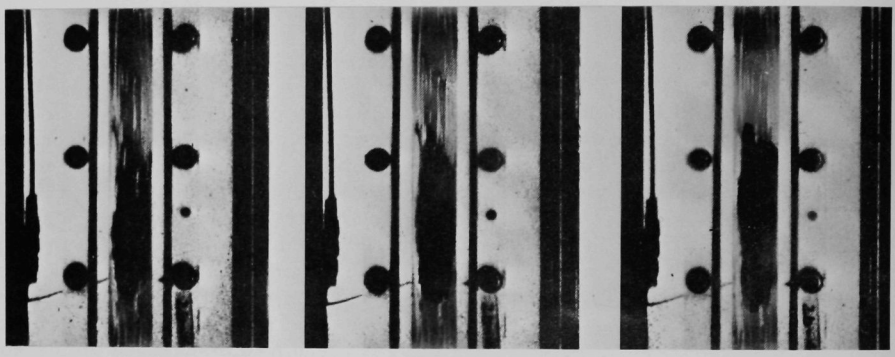

3 msec 4 msec 5 msec

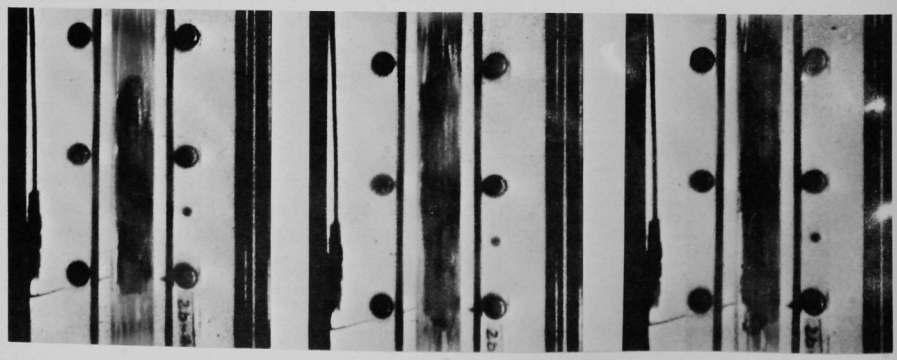

6 msec 7 msec 8 msec

Fig. 6. Sequence of Bubble Expansion at Various Time Intervals for Typical Transient. ANL Neg. No. 900-490.

IV. THE MATHEMATICAL MODEL

A. General Considerations

Consider a gas plenum of volume V, filled with gas at pressure P_{g_0}. At time t = 0, the cladding ruptures and the gas is released at such a rate (which depends upon the size and position of the clad rupture, the number of pins failed, and pressure and temperature of the gas in the plenum prior to rupture) that the ejected gas spreads out uniformly in all subchannels of the fuel assembly and subsequently expands axially as a single large bubble. In view of the fact that the density of the gas phase is very small compared to that of the liquid phase, the inertia and frictional effects of the gas phase, as compared to those of the liquid phase, may be neglected; it then follows from the momentum equation that the pressure within the gas-phase region is uniform. The thermal diffusivity of the gas is large compared to that of the coolant; for water as a coolant, as in these experiments, the thermal diffusivity of the gas is several times larger than that of water. The thermal diffusivity of the gas (at about 1000°F) is about three to four times as large as for liquid metals. It then follows from the energy equation that the temperature within the gas bubble may be taken as approximately uniform. For uniform pressure and temperature, the equation of state $P = \rho RT$ indicates that the density within the gas bubble may be taken to be uniform.

1. Governing Equations for Liquid Phase

The one-dimensional continuity and momentum relations for an infinitesimal fluid volume, assuming the flow to be incompressible (justification for this assumption is given later), are

$$\frac{\partial uA}{\partial x} = 0 \tag{1}$$

and

$$\frac{\partial u}{\partial t} + u\frac{\partial u}{\partial x} = -\frac{1}{\rho}\frac{\partial P}{\partial x} - g - \frac{f}{D_h}\frac{u|u|}{2}, \tag{2}$$

where u, ρ, and P are the cross-sectional averages of the longitudinal velocity, density, and pressure, respectively; A is the flow area; t is the time; x is the distance in axial direction; D_h is the hydraulic diameter; g is the acceleration due to gravity; f is the friction factor given by the formula

$$f = mRe^n, \tag{3}$$

where $Re = uD_h/\nu$; ν is the kinematic viscosity; and m and n are constants. It may be noted here that ρ and ν are evaluated at an average temperature (which, for example, for a reactor fuel assembly is equal to mean of the inlet and exit temperatures).

2. Governing Equations for Gas Phase

Let the pressure, density, and temperature of the gas in the gas plenum at any time be P_g, ρ_g, and T_g; let the corresponding values of these parameters in the gas bubble be P_b, ρ_b, and T_b. The application of conservation laws for a multiple pin failure gives the following relations: the law of mass conservation for the gas plenum

$$\frac{dV\rho_{gi}}{dt} = -Q_i I(t - t_i), \tag{4}$$

and the bubble

$$\frac{dA_c(X_u - X_L)\,\rho_b}{dt} = \sum_{i=1}^{N} Q_i I(t - t_i); \tag{5}$$

the law of energy conservation for the gas plenum

$$\frac{d\rho_{gi} V C_v T_{gi}}{dt} = -Q_i C_p T_{gi} I(t - t_i), \tag{6}$$

and the bubble

$$\frac{d\rho_b A_c(X_u - X_L)\,C_v T_b}{dt} + \frac{1}{J} P_b \frac{dA_c(X_u - X_L)}{dt} = \sum_{i=1}^{N} Q_i C_p T_{gi} I(t - t_i) + h\Delta TS, \tag{7}$$

where in writing the above equations it is assumed that the gas is ideal. In Eq. 6 it is implied that expansion of the gas in the gas plenum is adiabatic. In the above set of equations, subscript i refers to the pin i which ruptures at time t_i; N is the total number of pins ruptured; Q_i is the mass discharge rate from pin i; A_c is the effective flow area of the assembly; C_v and C_p are the specific heats of gas at constant volume and constant pressure, respectively; h is the film heat-transfer coefficient between the bubble and the surroundings; ΔT is the temperature difference between bubble and the surroundings; S is the effective surface area; X_u and X_L are the bubble coordinates (see Fig. 7); $I(t - t_i)$ is the unit step function defined as

$$I(t - t_i) = \begin{cases} 0 \text{ for } t < t_i \\ 1 \text{ for } t \geq t_i \end{cases},$$

where the rupture time t_i has the following specifications:

$$0 \leq t_i < t_r,$$

and where t_r is the initial transit time of the coolant for a single pass through the assembly. It may be noted here that, in the present state of the art, the exact failure mechanism for fuel elements is not yet known and, therefore, it becomes necessary that we should assume initiating occurrences that may lead to failure propagation. Consequently, depending upon the size of assembly and the initial coolant flow rate, we must assume the minimum number of pins ruptured and their rupture times so that "plug-type" bubble regime is established (see Eq. 31 below).

The rate Q_i of gas flow out of plenum i into bubble is, if the process of discharge is assumed quasi-stationary, equal to[11]

$$Q_i = C_{di} A_{0i} \rho_{gi} \left(\frac{P_b}{P_{gi}}\right)^{1/\gamma} \sqrt{\frac{2\gamma}{\gamma - 1}\left[1 - \left(\frac{P_b}{P_{gi}}\right)^{(\gamma-1)/\gamma}\right] R T_{gi} g_c} \qquad (8)$$

$$\text{for } \frac{P_b}{P_{gi}} \geq \left(\frac{2}{\gamma + 1}\right)^{\gamma/(\gamma-1)},$$

and

$$Q_i = C_{di} A_{0i} \rho_{gi} \left(\frac{2}{\gamma + 1}\right)^{1/(\gamma-1)} \sqrt{\frac{2\gamma}{\gamma + 1} R T_{gi} g_c} \qquad (9)$$

$$\text{for } \frac{P_b}{P_{gi}} \leq \left(\frac{2}{\gamma + 1}\right)^{\gamma/(\gamma-1)},$$

where A_{0i} is the area of breach in pin i; C_{di} is the coefficient of discharge; R is the gas constant; and $\gamma = C_p/C_v$. In the first case (Eq. 8), the flow is subcritical; and in the second case (Eq. 9), it is critical.

B. Application to Reactor Configuration and Conditions

In a reactor subassembly-configuration (shown in Fig. 7) the coolant enters from the inlet plenum, goes through the inlet piece into the test section, and exits into the outlet plenum through the transition piece. Since the expulsion process, as induced by rapid gas release or sudden vaporization of the superheated coolant, is highly inertia-dominated and the transient times of the event are very short, the inertial contribution of the fluid beyond the ends of the subassembly must also be taken into account.

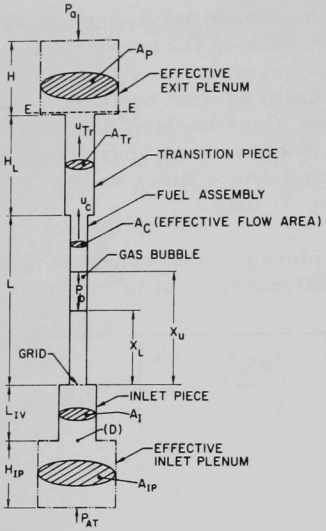

Fig. 7

Description of Coordinate System for Reactor-subassembly Configuration. ANL Neg. No. 900-564.

1. Motion of the Upper Gas-Liquid Interface

The integration of Eq. 2 together with the use of Eq. 1 between the upper gas-liquid interface and section E-E (see Fig. 7), including in the resulting expression the pressure-loss terms for sudden expansion both at the exit of subassembly and section E-E, yields

$$\frac{\rho}{g_c}\left(L - X_u + \frac{A_c}{A_{Tr}} H_L\right)\frac{d^2X_u}{dt^2} = P_b - P_E - \rho\frac{g}{g_c}(L - X_u + H_L)$$

$$+ \rho\frac{u_c|u_c|}{2g_c}\left[1 - \left(\frac{A_c}{A_{Tr}}\right)^2 - \left(\frac{A_c}{A_{Tr}}\right)^2\left(f_{Tr}\frac{H_L}{D_{Tr}} + K_E\right) - K_{Tr} - f_u\frac{L - X_u}{D_h}\right], \quad (10)$$

where P_E is the pressure at section E-E; g_c is the dimensional conversion factor; f_{Tr} is the friction factor for transition piece (or outlet zone), and f_u, the friction factor for the subassembly, is a function of Reynolds number (through Eq. 3) based on the velocity of the upper slug in the subassembly; K_E is the pressure-loss coefficient at section E-E and is given by expression

$$K_E = \left(1 - \frac{A_{Tr}}{A_p}\right)^2;$$

K_{Tr} is the pressure-loss coefficient at the subassembly exit and is given by expression

$$K_{Tr} = \left(1 - \frac{A_c}{A_{Tr}}\right)^2;$$

D_{Tr} is the diameter of the transition zone (shown in Fig. 7); D_h is the hydraulic diameter of the subassembly.

In the derivation of Eq. 10, the following boundary condition at the upper gas-liquid interface has been used:

$$u_c = \frac{dX_u}{dt},$$

and the pressure in the gas bubble is equal to the pressure in the fluid at the gas-liquid interface.

2. Inertial Contribution of Fluid in the Exit Plenum

As the fluid in the upper slug begins to be accelerated by the expanding gas bubble, the fluid in the transition piece (or outlet zone) at the inlet to the exit plenum assumes a "jet" action in almost "stationary" fluid in the plenum. This results in exchange of the momentum of the incoming fluid with the stationary fluid of the plenum. As a consequence of this large transition in the cross-sectional area at the exit of transition piece, the resulting flow in the plenum can no longer be considered to be one-dimensional and one cannot extend the use of Eq. 2 (one-dimensional description of the flow) to include the flow in the plenum. To handle this situation properly, the model should include the "effective" back pressure P_E at the exit of transition piece. This pressure in turn must be computed by assuming the flow in the plenum to be three-dimensional or, more simply, two-dimensional axisymmetric. Such an analysis of the flow in the plenum is presented in Ref. 12. The average pressure at the exit of transition piece is given by the following expression:

$$P_E(t) = P_a + \left[H\left(\frac{b}{a}\right)^2 + \frac{4}{a^2}\sum_{n=1}^{\infty}\frac{J_1^2(\alpha_n b)}{\alpha_n^3 J_0^2(\alpha_n a)}\right]\frac{\rho}{g_c}\frac{du_{Tr}}{dt}$$

$$- \frac{4b^2}{a^4}\frac{\rho}{g_c}\sum_{n=1}^{\infty}\frac{J_1^2(\alpha_n b)}{\alpha_n^2 J_0^4(\alpha_n a)}\left\{J_0^2(\alpha_n b) + J_1^2(\alpha_n b) - \frac{1}{\alpha_n b}J_0(\alpha_n b)J_1(\alpha_n b)\right\}u_{Tr}^2 \qquad (11)$$

(Contd.)

$$- \frac{8b}{a^4}\frac{\rho}{g_c}\sum_{m=1}^{\infty}\sum_{n=m+1}^{\infty}\frac{J_1(\alpha_m b)J_1(\alpha_n b)}{\alpha_m\alpha_n(\alpha_m-\alpha_n)\,J_0^2(\alpha_m a)J_0^2(\alpha_n a)}\{J_0(\alpha_n b)J_1(\alpha_m b) - J_0(\alpha_m b)J_1(\alpha_n b)\}\,u_{Tr}^2$$

$$- \frac{4b^2\rho}{a^4 g_c}\sum_{n=1}^{\infty}\frac{J_1^2(\alpha_n b)}{\alpha_n^2 J_0^2(\alpha_n a)}\,u_{Tr}^2 + \frac{g}{g_c}\rho H, \qquad \text{(Contd.)} \quad (11)$$

where α_n is a positive root of the equation

$$J_1(\alpha_n a) = 0;$$

b is the radius of the transition piece; H is the height of liquid column in the plenum; P_a is the pressure on the top of the plenum; u_{Tr} is the velocity of fluid in the transition piece related to the velocity in fuel subassembly through continuity Eq. 1; a is the radius of equivalent plenum which is associated with a single subassembly.

3. Motion of Lower Gas-Liquid Interface

The integration of Eq. 2, with the use of Eq. 1, between lower gas-liquid interface and the section through point D (see Fig. 7) gives us

$$\frac{\rho}{g_c}\left(X_L + L_{IV}\frac{A_c}{A_I}\right)\frac{d^2X_L}{dt^2} = P_D - P_b - \rho\frac{g}{g_c}(L_{IV}+X_L)$$

$$+ \frac{\rho u_L|u_L|}{2g_c}\left[\left(\frac{A_c}{A_I}\right)^2 - 1 - K_G - K_c - f_L\frac{X_L}{D_h} - f_I\frac{L_{IV}}{D_I}\left(\frac{A_c}{A_I}\right)^2\right]. \quad (12)$$

In the above equation P_D is the pressure at D; D_I is the diameter of the inlet zone; f_I is the friction factor and is a function of velocity in the inlet zone; f_L is a friction factor based on the velocity of the lower slug in the subassembly. Included in the above equation are the pressure-loss terms for the grid and for a sudden contraction (if the flow does not reverse in the lower slug during the transient) or sudden expansion (if the flow reversal takes place in lower slug during the transient). The loss coefficient K_c for a sudden contraction is given by

$$K_c = \frac{1}{2}\left(1 - \frac{A_c}{A_I}\right);$$

for sudden expansion it is given by

$$K_c = \left(1 - \frac{A_c}{A_I}\right)^2 .$$

The method for calculating the loss coefficient K_G for the grid is given in Ref. 13.

4. Inertial Contribution of Fluid in the Inlet Plenum

In the rapid gas release regime, if gas release rates are such that the flow reversal does not take place, the fluid entering the inlet region from the inlet plenum experiences a "contraction" that is, more simply, an increase in velocity. This results in a positive contribution to the pressure gradient between the inlet plenum and inlet region. This positive contribution in the pressure gradient tends to reduce the three-dimensionality effect discussed previously in relation to the exit plenum (this situation is somewhat analogous to the development of incompressible boundary-layer flow under pressure gradients). Consequently, if flow reversal does not take place during a transient, it may be adequate to describe the flow in the inlet plenum by one-dimensional continuity and momentum equations (Eqs. 1 and 2). For this case the pressure P_D is given by

$$P_D(t) = P_{AT} - \rho \frac{g}{g_c} H_{IP} - \rho \frac{H_{IP}}{g_c} \frac{A_c}{A_{IP}} \frac{d^2X_L}{dt^2} + \frac{\rho u_L |u_L|}{2g_c}\left[\left(\frac{A_c}{A_{IP}}\right)^2 - \left(\frac{A_c}{A_I}\right)^2 - \frac{1}{2}\left(1 - \frac{A_I}{A_{IP}}\right)\left(\frac{A_c}{A_I}\right)^2\right], \quad (13)$$

where the symbols used are defined in Fig. 7. However, if the flow reversal takes place, the flow "pattern" in the inlet plenum is identical to that in the exit plenum and therefore is treated similarly; the pressure P_D is given by expression which is identical to Eq. 11 except for the sign convention. The gravitational term must appear with a negative sign and the velocity downward (i.e., into the plenum) must be considered positive.

5. Resolution of Equations for Gas Bubble

In Eq. 7, the film heat-transfer coefficient h for the interface between the surroundings and bubble is not known, and any estimate of it may suffer from considerable uncertainties (e.g., due to lack of knowledge of the two-phase structure of interface regions). In view of this it may be adequate to replace the energy equation for the expansion of the bubble by the assumption that gas in the bubble expands isothermally. The validity of this assumption will be judged on the basis of the degree of agreement between the theoretical predictions and the experimental data.

From Eqs. 4 and 6 we obtain

$$\frac{T_{gi}}{T_{go}} = \left(\frac{\rho_{gi}}{\rho_{go}}\right)^{\gamma - 1}, \quad (14)$$

and the solution of Eq. 4 yields

$$\rho_{gi} = -\frac{1}{V}\int_{t_i}^{t} Q_i \, dt + \rho_{g0}, \tag{15}$$

which, for critical flow through the breach (i.e., Q_i is given by Eq. 9), becomes

$$\rho_{gi} = \left[\alpha(t - t_i) + \rho_{g0}^{(1-\gamma)/2}\right]^{2/(\gamma-1)} \tag{16}$$

where

$$\alpha = \frac{A_{0i}}{V} C_{di} \frac{\gamma - 1}{2}\left[\rho_{g0}^{(1-\gamma)/2}\right]\left(\frac{2}{\gamma + 1}\right)^{1/(\gamma-1)} \sqrt{\frac{2\gamma}{\gamma + 1} R T_{g0} g_c},$$

and T_{g0} and ρ_{g0} are the initial temperature and density of the gas in a gas plenum.

Combination of Eqs. 4 and 5 gives

$$A_c\rho_b(X_u - X_L) - A_c\rho_{b0}(X_{u0} - X_{L0}) = NV\rho_{g0} - \sum_{i=1}^{N} V\rho_{gi}, \tag{17}$$

where ρ_{b0} is the initial density of gas in the bubble at the initial system pressure at the point of breach; $X_{u0} - X_{L0}$ is the initial nonzero fictitious length of the bubble. This initial length of the bubble has been introduced to avoid the problem becoming indeterminate (to be described later) at time $t = 0$. Since introduction of this quantity represents a source of error, it is therefore chosen as close to zero as possible to keep the error a minimum. The above equation, when combined with the following equation (for isothermal expansion):

$$P_b = \rho_b \frac{P_{b0}}{\rho_{b0}}, \tag{18}$$

yields

$$P_b = \frac{P_{b0}}{\rho_{b0} V_b}\left[\rho_{b0} V_{b0} + NV\rho_{g0} - \sum_{i=1}^{N} V\rho_{gi}\right]. \tag{19}$$

In the above set of equations, P_{b0} is the initial pressure in the bubble and is approximately (surface-tension effects are neglected) equal to system

pressure at the location of the breach; V_b is the bubble volume at any time t; and V_{b0} is the initial volume of the bubble. From Eq. 19 it is clear that if V_{b0} is set equal to zero, the problem becomes indeterminate; thus the need for choosing a nonzero positive value for V_{b0} or $X_{u0} - X_{L0}$. In order to determine P_b, Eq. 19 is solved in conjunction with Eqs. 10, 12, and 16 for critical flow through a breach, or Eq. 15, with Q_i given by Eq. 8, for subcritical flow through a breach.

C. Application to Water Out-of-Pile Configuration and Conditions

Generally, in most simulation loops both in- and out-of-pile, only a limited bypass flow is provided, because of the limited capacity of the pumps used; furthermore, the inlet and exit plenums generally are not adequately simulated. This, in turn, implies that such reactor conditions as constant inlet pressure, P_{AT} (see Fig. 7), and inertial lengths beyond the pin assembly are not achieved in most simulation loops. The present water out-of-pile loop suffers from all above-mentioned shortcomings, which must be allowed for in the predictive model.

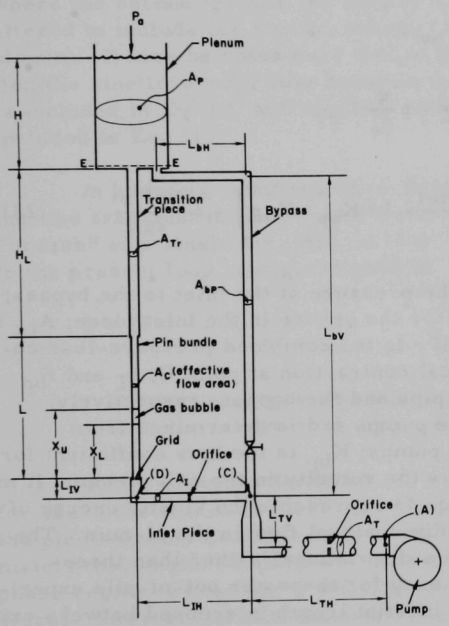

Fig. 8. Description of Coordinate System for Water Out-of-Pile Loop Configuration. ANL Neg. No. 900-543.

With the above in view, equations of motion of gas-liquid interfaces are extended to include (i) the inertial column between the branch-point C of the bypass (see Fig. 8) and the point D, (ii) the effect of "finiteness" of the bypass flow, and (iii) the pressure-flow characteristics of the pumps.

For the configuration of the simulation loop shown in Fig. 8, Eq. 12 is equally applicable, and Eq. 10 is applicable with slight modification (to be discussed later), except that now pressures P_D and P_E are obtained by solving the following set of equations. For the fluid column between points C and D, we have

$$P_D(t) = P_c(t) - \rho \frac{L_{IH}}{g_c} \frac{A_c}{A_I} \frac{du_L}{dt} - \rho \frac{u_L |u_L|}{2 g_c} \left[\left(\frac{A_c}{A_I} \right)^2 \left(f_I \frac{L_{IH}}{g_c} + K_{or} \right) \right]; \qquad (20)$$

between points C and A we have

$$P_c(t) = P_{AT}(t) - \rho \frac{g}{g_c} L_{TV} - \rho \frac{u_T |u_T|}{2g_c} \left[\left(\frac{A_T}{A_{cc}} \right)^2 - 1 + K_T + f_T \frac{L_{TV} + L_{TH}}{D_T} \right]$$

$$- \rho \frac{L_{TH} + L_{TV}}{g_c} \frac{du_T}{dt}, \tag{21}$$

where the total velocity u_T is obtained by

$$u_T = (A_c u_L + u_{bp} A_{bp}) / A_T \tag{22}$$

and the bypass velocity u_{bp} is given by

$$\rho \frac{L_{bV} + L_{bH}}{g_c} \frac{du_{bp}}{dt} = P_c - P_E - \rho \frac{g}{g_c} L_{bV}$$

$$- \rho \frac{u_{bp} |u_{bp}|}{2g_c} \left(f_{bp} \frac{L_{bV} + L_{bH}}{D_{bp}} - 1 + K_{bp} + K_{bE} \right) - \rho \frac{u_p |u_p|}{2g_c}. \tag{23}$$

In the above set of equations, P_c is the pressure at the inlet to the bypass; K_{or} is the pressure-loss coefficient for the orifice in the inlet piece; A_{cc} is the cross-sectional area at point C; K_T is the combined pressure-loss coefficient for the orifice and the gradual contraction at point C; f_T and f_{bp} are the friction factors for the main pipe and the bypass, respectively; P_{AT} is the pressure at the exit of the pumps and is determined from pressure-flow characteristics of the pumps; K_{bp} is the loss coefficient for the variable constriction (valve); u_p is the velocity in the exit plenum. It may be noted here that the last term in Eq. 23 represents the kinetic energy of the fluid in the plenum based on one-dimensional flow in the plenum. The reason for assuming the flow to be one-dimensional rather than three-dimensional is that the configuration used for the water out-of-pile experiment (see Fig. 8) had a considerable inertial length interposed between exit of the pin assembly and inlet of the exit plenum; its contribution outweighed the three-dimensional effects of the flow in the plenum. In view of the above discussion, the following equations are used to describe the flow in the exit plenum. These are

$$A_p u_p = A_c u_c + u_{bp} A_{bp} \tag{24}$$

and

$$P_E(t) = P_a + \rho \frac{H}{g_c} \frac{du_p}{dt} + \rho \frac{u_p |u_p|}{2g_c} f_p \frac{H}{D_p} + \rho \frac{g}{g_c} H, \tag{25}$$

where f_p is the friction factor for the plenum, and P_a is the pressure at the top of fluid in the plenum. In addition, Eq. 10, which describes the flow between upper gas-liquid interface and section E-E, is modified as follows:

$$\frac{\rho}{g_c}\left(L - X_u + \frac{A_c}{A_{Tr}} H_L\right) \frac{d^2X_u}{dt^2} = P_b - P_E - \rho\frac{g}{g_c}(L - X_u + H_L)$$

$$+ \rho\frac{u_c|u_c|}{2g_c}\left[1 - \left(\frac{A_c}{A_p}\right)^2 - \left(\frac{A_c}{A_{Tr}}\right)^2\left(f_{Tr}\frac{H_L}{D_{Tr}} + K_E\right) - K_{Tr} - f_u\frac{L - X_u}{D_h}\right], \quad (26)$$

where the second term in the square bracket on the right-hand side has been altered to include the kinetic-energy loss between pin assembly and the plenum. It may be noted here that in the analysis for the reactor configuration the kinetic-energy loss between the fuel assembly and the outlet region is included in Eq. 10, and the loss between outlet zone and the plenum is included in Eq. 11.

In adapting equations describing expansion of the gas bubble, we note that the transient in the present water out-of-pile experiment is initiated by "breach" of a single pin; this, in turn, implies that Eqs. 4 to 19 are applied to the present loop configuration with

$$i = N = 1; \; t_i = 0.$$

V. QUANTITATIVE CRITERION FOR VALID APPLICATION OF THE ANALYTICAL MODEL

From previous discussions, it is clear that the quantitative criterion for which the model is valid must satisfy the following: The flow regime in the pin assembly associated with the rapid gas release must be approximately that of two "separated" phases (i.e., the void fraction in the gas-phase region is near 100% and this region is confined between two liquid slugs). Interpreted mathematically, the above statement of the problem becomes

$$\sum_{i=1}^{k} Q_i(0)/\rho_{b0} \geq U_0 A_c, \quad (27)$$

where $Q_i(0)$ is the mass discharge rate of gas from a pin i at t = 0; U_0 is the initial coolant velocity in the pin assembly; k is the number of pins breached at t = 0.

As discussed previously, the gas release rate from a pin is a function of pressure and temperature of the fission gas in the plenum of the fuel element, and the size and location of the breach in the cladding. If the breach is located in the core region, then in addition to the above parameters the gas release rate is also a function of the porosity and the associated impedance to the flow of gas. Since at present no experimental data are available on the porosity or permeability and on the nature of pores in the fuel region, no definite estimates of internal frictional pressure drop can be made. However, in the present investigation, we assume that the internal resistance to the gas flow is negligible; this assumption is certainly valid if the breach is located in the gas-plenum region or in its close vicinity.

For a gas-plenum pressure of about 1000 psia and a system pressure of, say, 100 psia, $P_{b0}/P_{g0} \simeq 0.1$, which is well below the critical pressure ratio (~ 0.48); therefore, for most liquid-metal breeder reactors it is valid to assume that the initial gas discharge through any breach of finite size is critical. In view of the above assumption, the use of Eq. 9 in Eq. 27 gives

$$\left(\frac{2}{\gamma+1}\right)^{1/(\gamma-1)} \sqrt{\frac{2\gamma}{\gamma+1}}\, \rho_{g0} \frac{\sqrt{g_c R T_{g0}}}{\rho_{b0}} \sum_{i=1}^{k} C_{di} A_{0i} \geq U_0 A_c. \tag{28}$$

By replacing ρ_{g0} by P_{g0}/RT_{g0} and ρ_{b0} by P_{b0}/RT_{b0}, and assuming that the temperature of the gas in the plenum is equal to the temperature of the coolant outside the plenum, we obtain from Eq. 28 the following general criterion for conditions for which the analytical model is valid:

$$\sum_{i=1}^{k} C_{di} A_{0i} \geq \beta \frac{P_{b0}}{P_{g0}} \frac{U_0 A_c}{\sqrt{R T_{b0} g_c}}, \tag{29}$$

where

$$\frac{1}{\beta} = \left(\frac{2}{\gamma+1}\right)^{1/(\gamma-1)} \sqrt{\frac{2\gamma}{\gamma+1}}.$$

If all breached pins have the same breach size, A_0, and the same coefficient of discharge, C_d, Eq. 29 simplifies to

$$A_0 \geq \frac{\beta}{k C_d} \frac{P_{b0}}{P_{g0}} \frac{U_0 A_c}{\sqrt{R T_{b0} g_c}}, \tag{30}$$

which for a circular breach becomes

$$d \geq \left(\frac{4}{\pi} \frac{\beta}{kC_d} \frac{P_{b0}}{P_{g0}} \frac{U_0 A_c}{\sqrt{RT_{b0} g_c}} \right)^{1/2} . \qquad (31)$$

VI. COMPUTATIONS AND DISCUSSION OF RESULTS

A. The Water Out-of-Pile Simulation Loop

The relevant parameters such as pressure-loss coefficients, friction factors, and pressure-flow pump characteristics pertaining to the water out-of-pile simulation loop shown in Fig. 8 were determined experimentally. The initial conditions for starting computation were first determined for a given initial flow through the test section, from steady-state solution of Eq. 12 and Eqs. 20-26. These conditions include computation of the system pressure at the center of test section (the location of the "breach"), flow through the bypass and pressure coefficient for the valve opening in the bypass from the tabulated data (graphical representation of which is shown in Fig. 9), and initial exit pressure P_{AT} of pump and the corresponding total flow; the last two parameters were merely obtained to verify pressure-flow characteristics (shown in Fig. 10) of the pumps. It may be noted here that for a steady-state solution for the flow in the loop whose pressure-loss characteristics are known, there are more equations available than the number of unknowns, and these additional equations can

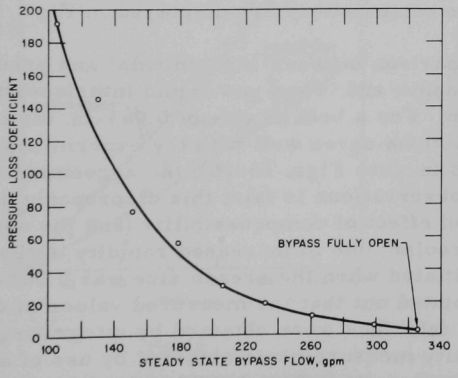

Fig. 9

Measured Distribution of Pressure-loss Coefficient of Variable Constriction (valve) in the Bypass as a Function of Steady-state Bypass Flow. ANL Neg. No. 900-541.

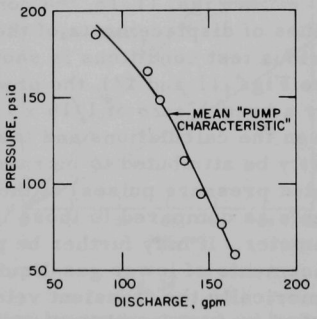

Fig. 10

Variation of Pressure at Exit of Pump with Pump Capacity. ANL Neg. No. 900-565.

be utilized to generate the pressure-flow characteristics of the pumps for various rates of flow through the test section. More specifically, we solve, for a given flow through the test section, the steady-state form of Eq. 25 to give P_E in terms of u_p or u_{bp} (see Eq. 24) which, when substituted into the steady-state form of Eq. 26, gives P_b in terms of u_{bp}. The substitution of P_b in terms of u_{bp} into the steady-state form of Eqs. 12 and 20 gives P_c in terms of u_{bp}. Finally, the steady-state form of Eq. 23, together with the data presented in Fig. 9, is solved iteratively to give u_{bp}. Having determined u_{bp}, we use Eq. 22 to determine u_T. Equation 21 then provides the corresponding value of P_{AT}. If the above process is repeated for a series of flow rates through the test section, we can then generate the pressure-flow characteristics of the pump. The pressure P_b so determined at $t = 0$ is utilized to calculate gas density ρ_{b0} from the equation of state, $\rho_{b0} = P_{b0}/RT_b$, where T_b is taken equal to the temperature of the coolant. The gas density of the bubble is then utilized to calculate the initial fictitious mass (as discussed previously) of gas in the bubble.

The solution of the dynamic (transient) problem was carried out by using the System/360 Continuous System Modeling Program (CSMP). For integration of the coupled differential equations, the fifth-order Milne predictor-corrector variable step-size routine (which is incorporated into CSMP) was used. The iterative procedure consisted in first determining the nature (critical or subcritical) of the gas discharge through a given size of breach; this, in turn, leads to the selection of the equation (see Eqs. 8 and 9) for calculating the discharge rate Q_i ($i = 1$). Equation 19 was then solved (iteratively) in conjunction with Eqs. 15, 12, and 20-26 and the pressure-flow characteristics to determine $P_{AT}(t)$ as a function of pump discharge. The results of these computations are displayed in Figs. 11-28.

In Figs. 11-16, the comparison between experimental and predicted values of displacements of the upper and lower gas-liquid interfaces for various test conditions is shown. For a breach size of 0.063-in. diameter (see Figs. 11 and 12), the predictions agree well with the experimental data. For a breach size of 1/16 x 1/8 in. (see Figs. 13-16), the agreement between the calculations and the observations is fair; this discrepancy may partly be attributed to increased effect of compressibility (and the associated pressure pulses) of the coolant due to increased rapidity of the transients as compared to those initiated when the breach size was 0.063-in. diameter. It may further be pointed out that the measured values of displacements of lower gas-liquid interface were obtained by integrating numerically the transient velocity measurements obtained by use of an orifice meter placed in the inlet piece (see Fig. 8). This inlet piece had three times as big a flow area as that of the 19-pin assembly; therefore, at low flow rates in the test section (e.g., 18 fps, which may reach a minimum of 9-11 fps in the test section during the transient), the flow rates through the inlet piece are even lower; the accuracy in measurement of low transient velocities in the inlet piece by means of an orifice meter becomes poor.[14]

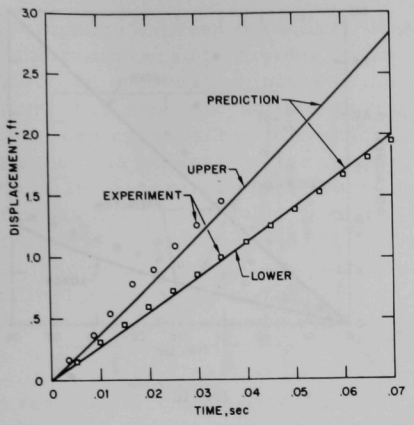

Fig. 11

Comparison between Experimental and Predicted Displacements of Upper and Lower Gas-Liquid Interfaces for Initial Test Conditions: Coolant Velocity = 30 fps; Gas-plenum Pressure = 515.0 psia; Breach Size = 0.063-in. Diameter. ANL Neg. No. 900-544.

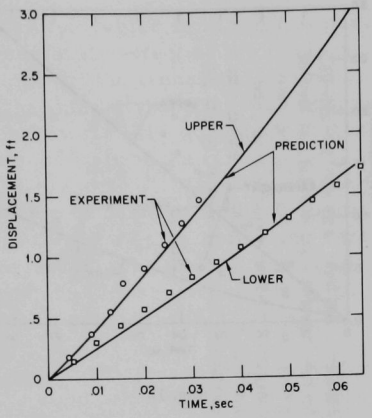

Fig. 12

Comparison between Experimental and Predicted Displacements of Upper and Lower Gas-Liquid Interfaces for Initial Test Conditions: Coolant Velocity = 30 fps; Gas-plenum Pressure = 1000.0 psia; Breach Size = 0.063-in. Diameter. ANL Neg. No. 900-546.

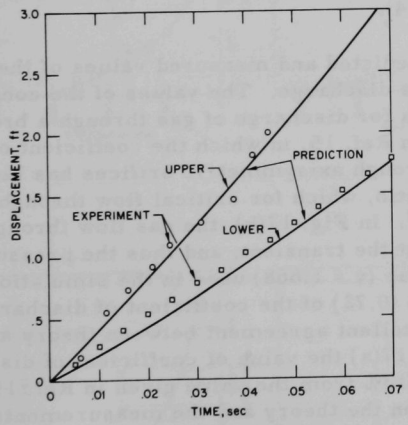

Fig. 13

Comparison between Experimental and Predicted Displacements of Upper and Lower Gas-Liquid Interfaces for Initial Test Conditions: Coolant Velocity = 28.0 fps; Gas-plenum Pressure = 665.0 psia; Breach Size = 1/16 x 1/8 in.^{2}. ANL Neg. No. 900-550.

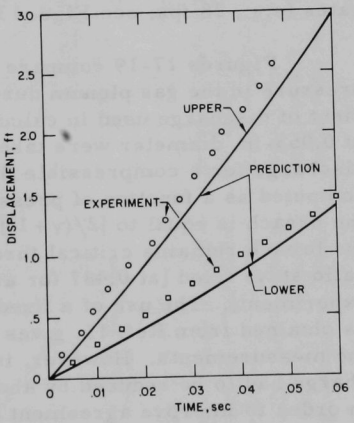

Fig. 14

Comparison between Experimental and Predicted Displacements of Upper and Lower Gas-Liquid Interfaces for Initial Test Conditions: Coolant Velocity = 28.0 fps; Gas-plenum Pressure = 995.0 psia; Breach Size = 1/16 x 1/8 in.^{2}. ANL Neg. No. 900-545.

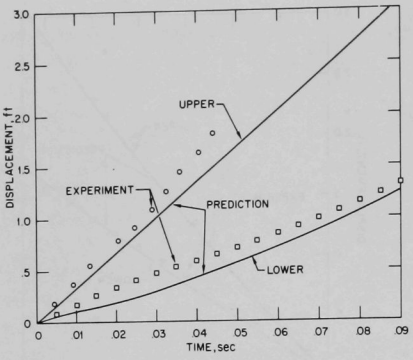

Fig. 15

Comparison between Experimental and Predicted Displacements of Upper and Lower Gas-Liquid Interfaces for Initial Test Conditions: Coolant Velocity = 18.0 fps; Gas-plenum Pressure = 665.0 psia; Breach Size = 1/16 x 1/8 in.^{2}. ANL Neg. No. 900-549.

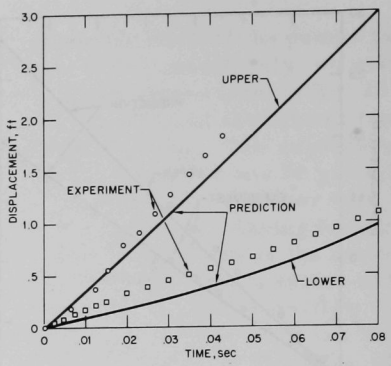

Fig. 16

Comparison between Experimental and Predicted Displacements of Upper and Lower Gas-Liquid Interfaces for Initial Test Conditions: Coolant Velocity = 18.0 fps; Gas-plenum Pressure = 835.0 psia; Breach Size = 1/16 x 1/8 in.^{2}. ANL Neg. No. 900-548.

This may explain the increased differences between the predicted and the measured values of displacements of the lower gas-liquid interface at lower flow rates (e.g., 18 fps; see Figs. 15 and 16) as compared to higher flow rates (e.g., 28 fps; see Figs. 13 and 14).

Figures 17-19 compare the predicted and measured values of the pressure in the gas plenum during gas discharge. The values of the coefficient of discharge used in calculations for discharge of gas through a breach of 0.063-in. diameter were taken from Ref. 15, in which the coefficient of discharge for a compressible flow through axisymmetric orifices has been computed as a function of pressure ratio, which for critical flow through the breach is equal to $[2/(\gamma+1)]^{\gamma/(\gamma-1)}$. In Fig. 17(b), the gas flow through the breach remains critical throughout the transient, and thus the pressure ratio stays fixed [at 0.487 for argon gas (γ = 1.668) used in the simulation experiment]. The use of a fixed value (0.72) of the coefficient of discharge, as obtained from Ref. 15, gives an excellent agreement between theory and the measurements. However, in Fig. 17(a) the value of coefficient of discharge had to be reduced by about 10-13% from the value given in Ref. 15 in order to improve agreement between the theory and the measurements. For a rectangular breach, there are no data available for the coefficient of discharge and, therefore, the value had to be chosen somewhat arbitrarily to carry out the calculations. It was found that a value of 0.5 produced an excellent agreement between the theory and the data (see Figs. 18 and 19).

Figures 20-22 compare the predicted and the measured transient pressures at three different axial locations in the test section; the large

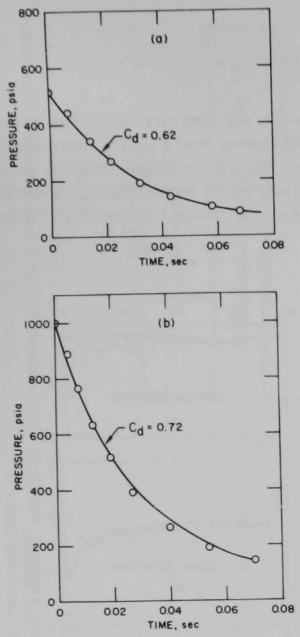

Fig. 17

Temporal Variation of Pressure in Gas Plenum during Gas Discharge for Initial Test Conditions: Coolant Velocity = 30.0 fps; Breach Size = 0.063-in. Diameter. (a) Gas-plenum pressure = 515 psia; (b) Gas-plenum pressure = 1000 psia. ANL Neg. No. 900-556.

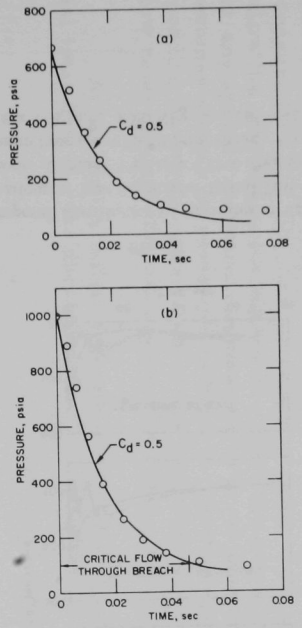

Fig. 18

Temporal Variation of Pressure in Gas Plenum during Gas Discharge for Initial Test Conditions: Coolant Velocity = 28.0 fps; Breach Size = 1/16 x 1/8 in.^{2}. (a) Gas-plenum pressure = 665 psia; (b) Gas-plenum pressure = 995 psia. ANL Neg. No. 900-552.

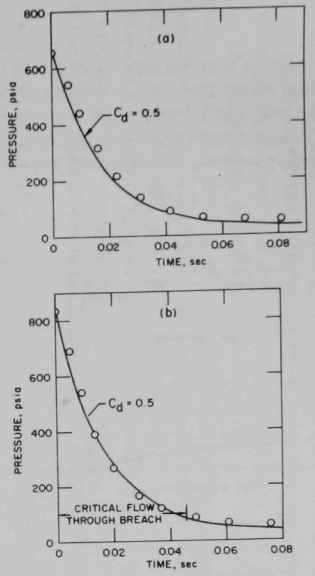

Fig. 19

Temporal Variation of Pressure in Gas Plenum during Gas Discharge for Initial Test Conditions: Coolant Velocity = 18.0 fps; Breach Size = 1/16 x 1/8 in.^{2}. (a) Gas-plenum pressure = 665 psia; (b) Gas-plenum pressure = 835 psia. ANL Neg. No. 900-547.

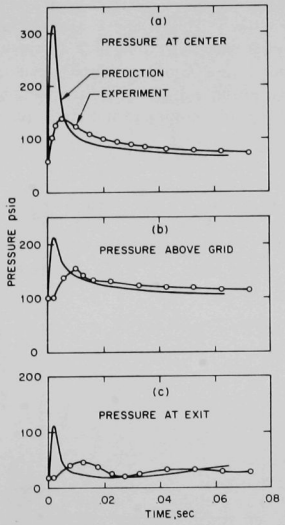

Fig. 20

Temporal Distribution of Pressures at Various Locations in Test Section for Initial Test Conditions: Coolant Velocity = 30.0 fps; Gas-plenum Pressure = 1000.0 psia; Breach Size = 0.063-in. Diameter. ANL Neg. No. 900-553 Rev. 1.

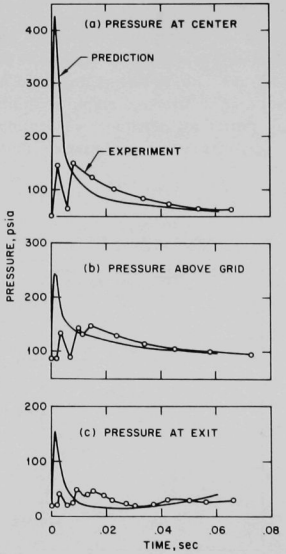

Fig. 21

Temporal Distribution of Pressures at Various Locations in Test Section for Initial Test Conditions: Coolant Velocity = 28.0 fps; Gas-plenum Pressure = 995.0 psia; Breach Size = 1/16 x 1/8 in.^{2}. ANL Neg. No. 900-551.

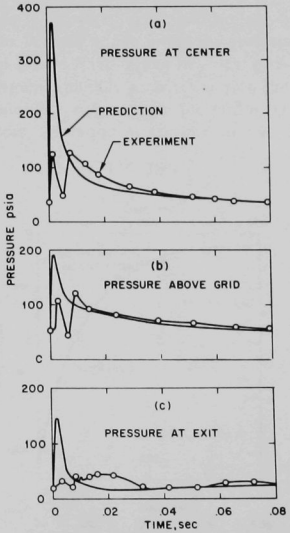

Fig. 22

Temporal Distribution of Pressures at Various Locations in Test Section for Initial Test Conditions: Coolant Velocity = 18.0 fps; Gas-plenum Pressure = 835.0 psia; Breach Size = 1/16 x 1/8 in.^{2}. ANL Neg. No. 900-566.

discrepancy between the measured and predicted values in the initial part of the transient is partly due to the compressibility effect of the coolant (which, of course, dominates in the initial part of the transient). Furthermore, it is expected that the maximum of the intensity of pressure occurs at the central breached pin during the initial burst of the gas, and it attenuates as the pressure pulse travels towards the wall of the test section, where the pressure pulses are measured. This attenuation in the intensity of pressure pulses is due to energy dissipation because of fluid viscosity, structural deformation, and reflection from the pins surrounding the central pin. However, in the later part of the transient, during which compressibility effects of the coolant are not as dominant, the agreement between the predictions and the measured values improves considerably.

Figures 23-25 show the calculated transient-pressure distributions at three different locations in the simulation loop. These figures clearly indicate that the constant "inlet" pressure condition, which is generally applicable in the reactor configuration, does not hold good in the present simulation loop. There is as much as 20% variation in the pump discharge pressure (see Fig. 25), and considerably more variation in the pressure below the grid and at the bypass inlet during a transient. The explanation for any specific difference between three cases presented in Figs. 23-25 becomes evident by reference to Figs. 26-28; the latter figures show corresponding (to pressure variation at the locations considered) variation of flow rates through the test section, the bypass, and the total-flow pipe.

At the higher initial coolant velocity of 30 fps (see Fig. 26), the initial total flow is considerably reduced as compared to initial total flow at

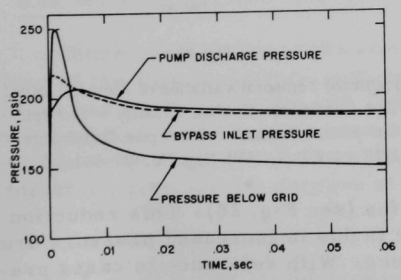

Fig. 23

Predicted Temporal Distribution of Pressures at Various Locations in Loop for Initial Test Conditions: Coolant Velocity = 30 fps; Gas-plenum Pressure = 1000.0 psia; Breach Size = 0.063-in. Diameter. ANL Neg. No. 900-559.

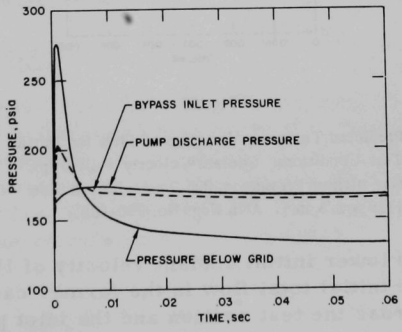

Fig. 24

Predicted Temporal Distribution of Pressures at Various Locations in Loop for Initial Test Conditions: Coolant Velocity = 28.0 fps; Gas-plenum Pressure = 995.0 psia; Breach Size = 1/16 x 1/8 in.^{2}. ANL Neg. No. 900-558.

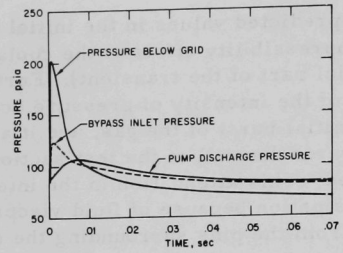

Fig. 25

Predicted Temporal Distribution of Pressures at Various Locations in Loop for Initial Test Conditions: Coolant Velocity = 18.0 fps; Gas-plenum Pressure = 835.0 psia; Breach Size = 1/16 x 1/8 in.^{2}. ANL Neg. No. 900-542.

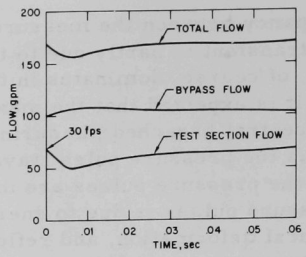

Fig. 26

Predicted Temporal Variation of Flow for Initial Test Conditions: Coolant Velocity = 30 fps; Gas-plenum Pressure = 1000.0 psia; Breach Size = 0.063-in. Diameter. ANL Neg. No. 900-560.

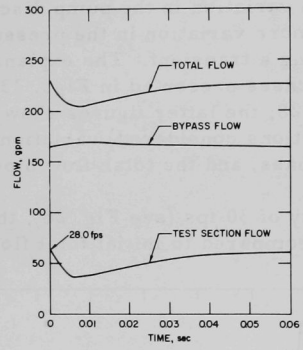

Fig. 27

Predicted Temporal Variation of Flow for Initial Test Conditions: Coolant Velocity = 28.0 fps; Gas-plenum Pressure = 995.0 psia; Breach Size = 1/16 x 1/8 in.^{2}. ANL Neg. No. 900-563.

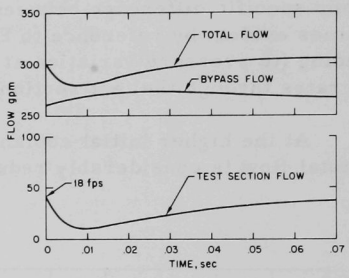

Fig. 28

Predicted Temporal Variation of Flow for Initial Test Conditions: Coolant Velocity = 18.0 fps; Gas-plenum Pressure = 835.0 psia; Breach Size = 1/16 x 1/8 in.^{2}. ANL Neg. No. 900-561.

the lower initial coolant velocity of 18 fps (see Fig. 28). This reduction in the initial total flow in the former case is due to increased pressure drop across the test section and the inlet piece. With reference to cases presented in Figs. 26 and 27, it may be noted that there is only a slight variation in the bypass flow (~2-3%), and the effect of reduction in test section flow is felt in the total flow and is reduced correspondingly. The explanation for this lies in the fact that the initial flow through the test section is controlled by varying the valve opening in the bypass and, at increased flows through the test section, a considerable pressure drop occurs across

the bypass. There exists only a small pressure drop across the total-flow pipe; consequently, any changes in the flow through the test section are directly reflected in the total flow. At low initial flow rates through the test section (see Fig. 28), the reduction in the flow through the test section during the transient is shared by increase in the bypass flow and the reduction in the total flow. It may be noted here that the relative amount of changes in flow through the bypass and the total-flow pipe during a transient are strictly function of the pressure-flow characteristics of the pumps and pressure-loss characteristics of the restrictions in the system.

Let us now apply the criterion given in Eq. 31 to test the applicability of the analytical model to the present simulation experiment. The values of the parameters that occur in Eq. 31 were taken as follows:

$$U_0 = 30 \text{ fps}; \quad A_c = 0.731 \text{ in.}^2; \quad P_{b0} = 56.7 \text{ psia};$$

$$P_{g0} = 1000 \text{ psia}; \quad k = 1; \quad C_d = 0.72; \quad T_{b0} = 530°R;$$

$$R = 38.66 \text{ ft-lb}_f/\text{lb}_m\text{-}°R; \quad \gamma = 1.668; \quad \beta = 1.377.$$

The substitution of the above values of the parameters in Eq. 31 yields

$$d \geq 0.061 \text{ in.}$$

Thus, according to the above criterion for initiating rapid gas release, the choice of a breach of 0.063-in. diameter in the simulation experiment was adequate for establishing the "plug-type" bubble regime, and good agreement between the measurements of the event and the predictions of the model provides to some extent indirect confirmation of Eq. 31.

B. Reactor Configuration and Conditions

Since comparison of the mathematical model with the measured values of the flow transients initiated in the simulation loop by a rapid gas release has confirmed principal applicability of the model, the model can now be applied to the fast-reactor configuration. The particular configuration chosen was that of the Fast Flux Test Facility (FFTF). The reactor parameters used for the purpose of the calculations are as follows:

Dimensions (in inches):

$$L = 96.0; \quad H_L = 24.0; \quad L_{IV} = 36.0;$$

$$H = 240; \quad D_h = 0.1281; \quad H_{IP} = 132;$$

$$A_c = 6.724; \quad A_{Tr} = A_I = 16.274; \quad V = 1.26.$$

The cross-sectional area of the equivalent plenum is found by utilizing the continuity equation under steady-state conditions. This gives us

$$N_A u_{Tr}(0) A_{Tr} = A_p u_p(0),$$

where N_A is the number of assemblies in the reactor. The above equation implies that the equivalent plenum (i.e., portion of the plenum associated with a single subassembly) must have a cross-sectional area equal to A_p/N_A. Based on 92 effective (those through which the coolant flows) subassemblies and a 20-ft diameter of the plenum, the above considerations gave us a cross-sectional area of the equivalent inlet and exit plenums of 491 in.^{2}.

Additional parameters:

Coolant velocity = 25.5 fps

Inlet temperature = 740°F

Outlet temperature = 1100°F

Cover-gas pressure = 14.7 psia

Gas-plenum pressure = 1000 psia.

The use of the above parameters and those obtained from steady-state solution of Eqs. 10-13 and 31 gave for the number of failed pins k = 10 and C_d = 0.62, the following criterion for the applicability of the model:

$$d \geq 0.067 \text{ in.}$$

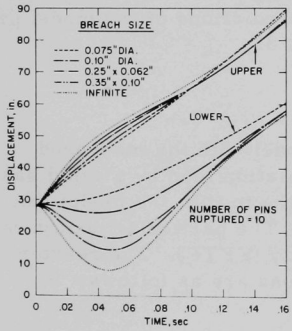

Fig. 29

Calculated Displacements of Upper and Lower Gas-Liquid Interfaces for FFTF Fuel Subassembly for Initial Conditions: Coolant Velocity = 25.5 fps; Gas-plenum Pressure = 1000.0 psia. ANL Neg. No. 900-555.

In obtaining this criterion, it was assumed that breaches in all pins occurred at 28.0 in. from the bottom of the pin assembly. The fuel resistance to the gas flow was neglected.

After having obtained the criterion for establishing the applicability of the model, the dynamic solution of Eqs. 10-13, 19, 15, and 8 or 9 (depending upon whether the flow through the breach was subcritical or critical) was obtained for various breach sizes. The results of the computations are displayed in Fig. 29. The calculations for "infinite" breach (i.e., the expansion of the gas is continuous and the pressure in the bubble is equal to plenum pressure for as long as the bubble stays in contact with the breach) were also carried out; the results are also shown in Figure 29. This figure indicates that the reversal of the flow begins to occur for breaches larger than 0.075 in. in diameter

for a rupture of 10 pins. For very large breach sizes flow reversal is almost "instantaneous," and it takes as much as 130 msec before the flow recovers back to normal. It may further be observed that there is considerably more spread in displacements of the lower gas-liquid interface as compared to the spread in displacements of the upper gas-liquid interface. This is mainly due to longer frictional and inertial lengths of the upper slug as compared to the lower slug. Furthermore, the presence of the instrument package near the top end of the pin assembly causes a considerable pressure drop (~15 psi at 25.5 fps). The combined effect of all these is to impede the expulsion of the upper slug. This impedance increases with the increase in velocity, and therefore the spread in displacements of the upper gas-liquid interface is not as much as it is for displacements of the lower gas-liquid interface.

VII. CONCLUSIONS

It would appear from the experiment that the flow transients induced by rapid gas release are of relatively short duration, so that it may be expected that the coolant flow will be reestablished prior to overheating of the adjacent fuel pins. However, the experiment did not simulate very closely the actual reactor conditions in several aspects. Therefore, the experimental data presented should not be taken as completely representative of what will happen under actual reactor conditions. Notwithstanding this, the experiment has reasonably achieved the objectives of (1) furnishing a good physical picture of the phenomena involved with rapid gas release and (2) providing the means for developing a mathematical model capable of predicting the flow transients in a reactor configuration, as well as in out-of-pile and in-pile test loops. In addition, the model developed can easily be applied to calculate voiding rates due to fission gas release in whole-core accidents. Best agreement between experiment and calculation was achieved for breach sizes which were only slightly larger than the minimum size required for valid application of the analytical model. For larger breach sizes, the discrepancy between the calculations and the experimental data was attributed to compressibility effects of the coolant resulting from the increased severity of the flow transients.

From the sample calculations presented for an FFTF fuel-subassembly configuration (with a simultaneous rupture of 10 pins and neglecting the resistance to the flow of gas internally in the fuel), the maximum gas-blanketing time was found to be ~100 msec. Calculations of clad-temperature transients (at the location of maximum linear heat rating) show that complete thermal insulation of a fuel pin for 100 msec will result in a rise of ~100°C. It would therefore appear that temperature transients due to rapid gas release caused by simultaneous rupture of as many as 10 pins do not lead to further clad failures.

The experimental and analytical work presented here indicates the following necessary areas for future effort:

1. Check the analytical model against experimental results to be obtained in a larger pin array, using a test loop which simulates more closely the actual reactor conditions.

2. Include compressibility effects of the coolant to improve agreement between the predictions and the data for breach sizes considerably larger than the minimum required for valid application of the model.

3. Extend the analytical model to a three-dimensional treatment of the case in which the gas bubble does not occupy the entire fuel-subassembly cross section.

It is expected that the work under items 2 and 3 will contribute to gaining a better understanding as to the possibility of fuel-failure propagation through mechanical loading effects due to pressure pulses.

ACKNOWLEDGMENTS

We would like to express our deep appreciation to Mr. Henry Halle for his work in the design of the piston valve assembly and the test section. Messrs. C. J. Roop and L. Bova are acknowledged for their excellent work in the design of much of the experimental apparatus and for their efforts in the collection of data. Many discussions with Dr. Hans K. Fauske and Messrs. Jan B. van Erp, John F. Marchaterre, Richard O. Ivins, Richard P. Anderson, Jack H. Tessier, and Dr. Ralph M. Singer are gratefully acknowledged. The help afforded by Messrs. Charles Fiala and Frank Del Angel in performing some of the computer calculations and preparing figures is gratefully acknowledged.

REFERENCES

1. B. M. Hoglund, R. P. Anderson, and L. Bova, *Experimental Study of a Gas Jet Penetrating a Liquid Coolant and Impinging on a Heated Surface*, ANL-7734 (to be published).

2. J. F. Koenig, Argonne National Laboratory, personal communication (Aug 1970).

3. M. Hori and A. J. Friedland, *Effect of Gas Entrainment on Thermal-hydraulic Performance of Sodium Cooled Reactor Core*, J. Nucl. Sci. Technol. *7*(5), 256-263 (May 1970).

4. M. Hori and A. J. Friedland, *Analysis of Gas-release Effect in Fuel Cladding Failure*, Trans. Am. Nucl. Soc. *12*(1), 333-334 (June 1969).

5. R. C. Noyes, H. Lurie, and A. A. Jarrett, "The Development and Growth of In-core Voids due to Boiling during Fast Reactor Transients," *Proceedings of the Conference on Safety, Fuels, and Core Design in Large Fast Power Reactors*, October 11-14, 1965, ANL-7120, pp. 881-889.

6. E. G. Schlechtendahl, *Theoretical Investigations on Sodium Boiling in Fast Reactors*, Nucl. Sci. Eng. *41*(1), 99-114 (July 1970).

7. W. D. Ford, H. K. Fauske, and S. G. Bankoff, to be published in Intern. J. Heat Mass Transfer.

8. M. A. Grolmes and H. K. Fauske, "Modeling of Sodium Expulsion with Freon-11," ASME Paper 70-HT-24, *ASME Heat Transfer Conference*, May 24-27, 1970.

9. K. Uematsu, K. Miyaguchi, Y. Kumaoka, and T. Uemura, *Experimental Study of the Consequences of Fuel Cladding Failure. Part II*, AFCPU-REPORT-023, p. 256, Atomic Fuel Corporation, Japan (1967).

10. S. Kondo, K. Miyaguchi, S. An, and A. Oyama, *A Simulation Experiment of the Results of Fission Product Gas Release due to Fuel Cladding Failure Using Water Circulation System*, J. Nucl. Sci. Technol. *7*(4), 197-209 (Apr 1970).

11. I. P. Ginzburg, *Applied Fluid Dynamics*, NASA-TT-F-94, pp. 222-224, Israel Program for Scientific Translations, Jerusalem (1963).

12. T. C. Chawla and B. M. Hoglund, *Pressure Distribution for Axisymmetric Two-dimensional Flow in a Plenum during Coolant Expulsion*, Nucl. Sci. Eng. *43*(1), 87-90 (Jan 1971).

13. I. E. Idel'chik, *Handbook of Hydraulic Resistance*, AEC-TR-6630, pp. 107-117, Israel Program for Scientific Translations, Jerusalem (1966).

14. T. G. Beckwith and N. Lewis Buck, *Mechanical Measurements*, 2nd ed., p. 423, Addison-Wesley Publishing Company, Mass. (1969).

15. J. Patterson, N. W. Page, and J. B. Ritchie, *Contraction Coefficients for Compressible Flow through Axisymmetric Orifices*, Int. J. Mech. Sci. *12*(5), 405-415 (May 1970).